

THREE VISION-BASED BEHAVIORS FOR SELF-POSITIONING A MOBILE ROBOT

Claudio Facchinetti, François Tièche and Heinz Hügli

(claudio.facchinetti@imt.unine.ch)

Institute of Microtechnology

University of Neuchâtel, Switzerland

Abstract. *This paper presents the analysis of vision-based homing behaviors that provide self-positioning of a mobile robot. The control schemes of the homing behaviors are based on a new approach that describes robot moves in terms of regulation by image features, hence avoiding the usual step of three-dimensional reconstruction of the scene with respect to the camera. Homing behaviors are the key elements of the self-positioning navigation approach we developed for our mobile robot, which basic idea is to represent the robot spatial knowledge in a topological map, where nodes consist in self-positioning sites and edges may be any behavior linking two nodes.*

Key Words. Mobile Robotics, Behavior-based Navigation, Self-Positioning, Vision-Based Control

1. INTRODUCTION

One of the problems autonomous mobile robots are confronting is representing and learning spatial knowledge in order to operate in a physical environment. A proposition for the body of this knowledge is the *cognitive map* (Connel and Mahadevan, 1993)(Kuipers and Byun, 1991), which may be analyzed in two ways. From the topological point of view (or *reasoning level*), the cognitive map is centered on a symbolic representation. From the robot resources point of view (or *control level*), the cognitive map is grounded in the interaction of the robot sensors and actuators with the environment.

The behavioral approach to control robots is inspired to some extent by the animal world, where a behavior may be described as an independent stereotyped action that is maintained by a specific stimulus. Simple tasks can be achieved very easily with behaviors moving the robot along a wall, avoiding unexpected obstacles or moving towards objects in the scene. However, a common problem is that typical navigation problems that require spatial knowledge (a topological map) are difficult to solve, since the robot underlying subsumption architecture (Brooks, 1986) is based on an interaction of the environment with reactive behaviors that are not mapped in the robot configuration space.

In the autonomous architecture we developed for our mobile robot, the control level consists of

robot moves to low-level visual primitives observed from the environment, such as points and segments extracted from image sequences (Müller *et al.*, 1993)(Hügli *et al.*, 1993). A solution to the spatial knowledge problem is provided by the self-positioning navigation approach we proposed in earlier publications (Facchinetti *et al.*, 1995)(Facchinetti *et al.*, 1994), which uses a new class of vision-based *homing* behaviors that provides the critical link between the reasoning and control levels. The homing behaviours control the robot moves so that they tend to match visual image features currently observed by a camera against a predefined target image. As a result, *homing sites* are created in areas of the environment where image features may stimulate a homing behaviour.

At the reasoning level, the homing sites are symbolized by nodes, while all the other reactive behaviors are represented by edges (Tièche *et al.*, 1994)(Dudek *et al.*, 1991). A typical behavior linking two nodes is path-following using odometric sensors. Nodes and edges form a network that describe the spatial knowledge of the robot about its environment (see Figure 1). This topological map can be used to plan the robot actions, distinguish ambiguous sites and explore unknown areas of the environment.

We propose in this paper a more detailed study of the homing behaviors. A main concern that is addressed here is to characterize which image features and which control law to use in order to define stable homing sites, so that they may be

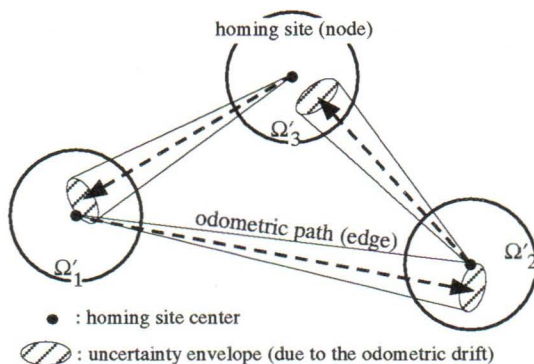


Figure 1 The robot is moving within and between homing sites (numbered 1 through 3) using, respectively, vision-based homing behaviors and path-following behaviors. The circles represent the capture zones of the homing behaviors.

used as navigation elements. We developed three homing behaviors, based on different vision systems, for evaluating the self-positioning concept on a real robot: homing on wall corners, homing on landmark pairs and homing on ceiling structures.

In the following Section, we briefly describe work in related domains. In Section 3, we present the vision-based control method used in the homing behaviors, as well as two examples of the type of image features they use. In Section 4, we detail three examples of homing behavior configurations. Experimental results for a preliminary implementation of the homing on landmark pairs are reported in Section 5. Finally, Section 6 concludes this paper.

2. RELATED WORK

The self-positioning approach contrasts with more traditional positioning (or localizing) approaches (Chenavier and Crowley, 1992)(Faugeras, 1993) that estimate the robot position by matching sensed features against a geometrical model of the environment using stereoscopy (2 or 3 cameras), dynamic vision (single mobile camera) or similar techniques (Takeda *et al.*, 1994). In the self-positioning approach, the three-dimensional reconstruction step is avoided since we do not use this information in the homing process, but instead control the robot moves directly in terms of regulation by image features.

The work presented in (Samson *et al.*, 1991) is a detailed study of the task function approach, which is reported in (Espiau *et al.*, 1992) for the particular case of vision sensor signals. The basic

idea of the control is to express changes in image features, such as points and lines, into changes in the camera moves with respect to the scene, in the neighborhood of a desired pose of the camera. The usual step consisting in estimating the three-dimensional pose of the object with respect to the camera is avoided. Experimental results are proposed for two vision task functions performed from points (target positioning) and lines (road following) in the image.

A form of homing navigation for a mobile robot is also used in (Tan *et al.*, 1991). The navigation of the robot is uniquely described in terms of homing sites, which capture regions intersect in the configuration space. The image feature defining a homing site consist in a snapshot of the world taken from that position.

3. PROBLEM STATEMENT

We present an analysis of vision-based homing behaviors, for which the control of the robot moves is directly achieved in terms of regulation in the image. The emphasis is on application and we present here the results without proofs. For a complete study of the control regulation we refer to other sources (Espiau *et al.*, 1992)(Samson *et al.*, 1991).

3.1 Robot geometry

The robot geometry is depicted in Figure 2. It is based on a synchronous drive mechanical system that provides zero gyro-radius (rotation without translation). The robot control space is two-dimensional and is described by $(\eta_1, \eta_2)^T$, where η_1 is the velocity in the heading direction and η_2 the angular velocity of the robot frame. The configuration space, however, is three-dimensional and is described by $(x, z, \theta)^T$. Hence, the robot can only translate along the forward and backward directions in which the three wheels are aligned, which is a non-holonomic constraint similar to that of a car.

The camera frame origin c is placed at a height h overhead the robot frame origin and is limited to a single rotation degree of freedom ϕ around the axis y of camera A (around the axis z of camera B), which gives a third control input $\eta_3 = \dot{\phi}$. The camera velocity with respect to the scene (frame 0) is described by $\dot{r}_c = (\dot{x}, \dot{z}, \dot{\phi})^T$ for camera A (by $\dot{r}_c = (\dot{x}, \dot{y}, \dot{\phi})^T$ for camera B).

The transform from camera velocity \dot{r}_c to robot velocity $\dot{r}_r = (\dot{x}, \dot{z}, \dot{\theta})^T$ is partially given by

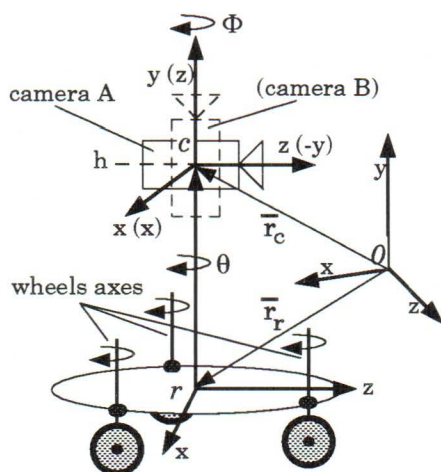


Figure 2 Nomad-200 robot geometry with two camera configurations A and B.

$$\begin{pmatrix} \dot{x}_r \\ \dot{z}_r \end{pmatrix} = \begin{pmatrix} \cos \phi & \sin \phi \\ -\sin \phi & \cos \phi \end{pmatrix} \cdot \begin{pmatrix} \dot{x}_c \\ \dot{z}_c \end{pmatrix} \quad (1)$$

for camera A (replace $(\dot{x}_c, -\dot{y}_c)^T$ for camera B). Finally, the robot control inputs (η_1, η_2) can be derived from the dynamic model of the robot described by

$$\begin{aligned} \dot{x} &= -\eta_1 \sin \theta \\ \dot{z} &= \eta_1 \cos \theta \\ \dot{\theta} &= \eta_2 \end{aligned} \quad (2)$$

Various approaches have been proposed for mobile robot control under non-holonomic constraints (Chacal and Sira-Ramirez, 1994)(d'Andréa-Novel et al., 1991)(Pissard-Gibollet and Rives, 1991) and their study is outside the scope of this paper. We propose in Section 5 a homing control implementation that simplifies the dynamic model.

3.2 Scene and image coupling

Without loss of generality we can consider a pin-hole camera model with unit focal length, so that the image projection $\bar{X}_i = (X_i, Y_i, 1)^T$ of a point $\bar{x}_i = (x_i, y_i, z_i)^T$ in three-dimensional space is given by $\bar{X}_i = 1/z_i \bar{x}_i$, which by temporal differentiation yields

$$\dot{\bar{X}}_i = \mathbf{L}_{\bar{X}_i} \dot{\bar{r}} \quad (3)$$

where the general expression of the *interaction matrix* $\mathbf{L}_{\bar{X}_i}$ for a 6x1 velocity vector $\dot{\bar{r}}$ (three translation and three angular velocities) is equal to

$$\begin{pmatrix} -1/z_i & 0 & X_i/z_i & X_i Y_i & -(1+X_i^2) & Y_i \\ 0 & -1/z_i & Y_i/z_i & 1+Y_i^2 & -X_i Y_i & -X_i \end{pmatrix} \quad (4)$$

It may be interesting to consider geometric image features obtained from the \bar{X}_i coordinates, such as straight lines or distances between image points. For this purpose, we define a *scene feature* \bar{p} as a set of three-dimensional geometrical primitives linked to a rigid object in the scene and the function $h(\bar{x}, \bar{p}) = 0$, which describes a specific configuration of \bar{p} . Correspondingly, the relation $g(\bar{X}, \bar{P}) = 0$ can be defined in the image frame, with \bar{P} obtained from \bar{p} by perspective projection (Espiau et al., 1992).

An *image feature vector* \bar{s} is then defined as the function $\bar{s} = f(\bar{P})$. In practice, \bar{s} is chosen so that $f()$ is a differentiable function of \bar{P} . A particularly interesting property is that if \bar{s} depends on the configuration of k different primitives (i.e. $\bar{s} = f(\bar{P}_1, \dots, \bar{P}_k)$), we have

$$\frac{\partial \bar{s}}{\partial \bar{r}} = \sum_{i=1}^k \frac{\partial \bar{s}}{\partial \bar{P}_i} \frac{\partial \bar{P}_i}{\partial \bar{r}} \quad (5)$$

Finally, from \bar{s} we define a *target image feature vector* \bar{s}^* , as equal to \bar{s} when the camera is at the desired pose with respect to the scene (the homing site center).

3.2 Examples of image features

a) Let \bar{m}_i be a point in the scene with coordinates \bar{x}_i . Consider the trivial case where \bar{p} is chosen as a chart-representation. We have $\bar{p} = \bar{x}_i$ and $\bar{P} = \bar{X}_i$. The interaction matrix is given by (4). Various other useful image features may be generated using this simple primitive: length and orientation of segments, mass center of a cluster of points, etc.

b) Let us consider a straight line specified by the intersection of two planes in the scene given by

$$h(\bar{x}, \bar{p}) : \begin{cases} a_1 x + b_1 y + c_1 z + d_1 = 0 \\ a_2 x + b_2 y + c_2 z + d_2 = 0 \end{cases} \quad (6)$$

The projection of $h(\bar{x}, \bar{p})$ in the image is described by the line equation $AX + BY + C = 0$. We choose the chart $\bar{P} = (\rho, \psi)$ to parametrize (A, B, C) , so that

$$g(\bar{X}, \bar{P}) = X \cos \psi + Y \sin \psi - \rho = 0 \quad (7)$$

It has been shown elsewhere (Espiau *et al.*, 1992) that the matrix \mathbf{L}_P can be written as equal to

$$\begin{pmatrix} \lambda_\psi c & \lambda_\psi s & -\lambda_\psi \rho & -\rho c & -\rho s & -1 \\ \lambda_\rho c & \lambda_\rho s & -\lambda_\rho \rho & (1+\rho^2)s & -(1+\rho^2)c & 0 \end{pmatrix}$$

$$\lambda_\psi = (a_i \sin \psi - b_i \cos \psi)/d_i$$

$$\lambda_\rho = (a_i \rho \cos \psi + b_i \rho \sin \psi + c_i)/d_i \quad (8)$$

with $s = \sin \psi$, $c = \cos \psi$ and choosing i such that $d_i \neq 0$.

3.3 Vision-based control

The control law we use for the homing behaviors is a simplification of the task function approach (Samson *et al.*, 1991) proposed by (Espiau *et al.*, 1992) for the specific case of visual sensor signals. The vision-based homing control can be expressed as the regulation to zero of a function \bar{e} , the main task, which is given by

$$\bar{e} = \mathbf{C}(t)[\bar{s}(\bar{r}_c, t) - \bar{s}^*(t)] \quad (9)$$

Since we are only interested in fixed image features ($\dot{\bar{s}}^* = 0$), the matrix \mathbf{C} is constant.

The basic idea for controlling the robot moves in terms of regulation by image features is to have the main task \bar{e} behaving like a first-order decoupled system

$$\dot{\bar{e}} = -\lambda \bar{e} = \frac{\partial \bar{e}}{\partial \bar{r}} \dot{\bar{r}}_c + \frac{\partial \bar{e}}{\partial t} \quad (10)$$

where $\lambda > 0$. Then, assuming scene features are motionless (Espiau *et al.*, 1992), the homing control law may be simplified to

$$\dot{\bar{r}}_c = -\lambda \bar{e} = -\lambda \mathbf{W}^+ \mathbf{C}[\bar{s}(\bar{r}_c, t) - \bar{s}^*(t)] \quad (11)$$

Where the rows of \mathbf{W} are made from the basis vectors of the camera configuration space and λ is a constant, which may be considered as a gain fixed according to the rate of the control loop. The size of \mathbf{W} is $m \times n$, where m is the dimension of \bar{e} and n is the number of camera degrees of freedom, which is equal to three in our case. The matrix product $\mathbf{W}\mathbf{W}^+$ may be chosen so that

$$w_{ij} = \begin{cases} 1 & \text{if } i = j = u, v, w \\ 0 & \text{otherwise} \end{cases} \quad (12)$$



Figure 3 Camera point-of-view of two scene features (reflective landmarks) used for homing the robot. A fisheye lens is used to increase the camera field of view

where the w_{ij} 's describe the components of the matrix product $\mathbf{W}\mathbf{W}^+$, with $u = 1$, $v = 3$ and $w = 5$ for camera A ($u = 1$, $v = 2$ and $w = 6$ for camera B). Convergence of the control law may be obtained even for an initial camera pose far away from the desired one.

The best convergence is obtained by choosing

$$\mathbf{C} = \mathbf{W}\mathbf{L}_{\bar{s}=\bar{s}^*}^+ \quad (13)$$

where $\mathbf{L}_{\bar{s}=\bar{s}^*}^+$ is the pseudo-inverse of the interaction matrix at the camera location corresponding to the desired image features $\bar{s} = \bar{s}^*$.

4. HOMING BEHAVIORS

We developed three homing behaviors for evaluating the self-positioning concept in a real world, using vision-based control. They use different image features and robot geometries to achieve the homing task.

4.1 Homing on landmark pairs

The homing on landmark pairs uses a vision device made of a grayscale video camera and a white fluorescent tube mounted on top of the robot (camera A in Figure 2). It allows to easily detect reflective landmarks disposed arbitrarily in the scene from their background (see Figure 3). A fast processing method based on bubble coloring and position prediction is then applied to track the corresponding two-dimensional targets in the image frame (Chantemargue and Hügli, 1994). The vision process time is about 40 ms.

The image features used for regulation consist in

the two targets specified by their mass centers $\bar{s} = (X_1, X_2, Y_1, Y_2)^T$. If the camera goal location is such that the image plane is parallel to the line supporting the landmarks, the target image features are given by $\bar{s}^* = (-a, a, a, a)^T$, where $a = l/2 z^*$, l being the distance between the two landmarks and z^* the desired range between the camera and the two landmarks. The matrix $\mathbf{L}_{\bar{s}\bar{s}^*}$ is derived from (4) and is equal to

$$\begin{pmatrix} -1/z^* & 0 & -a/z^* & -a^2 & -1-a^2 & a \\ -1/z^* & 0 & a/z^* & a^2 & -1-a^2 & -a \\ 0 & -1/z^* & a/z^* & 1+a^2 & a^2 & a \\ 0 & -1/z^* & a/z^* & 1+a^2 & -a^2 & -a \end{pmatrix} \quad (14)$$

Let us consider a numerical example with $l = 1 m$ and $z^* = 2 m$. By keeping only relevant terms, the control law (11) may be simplified to $\dot{\bar{r}}_c = (\dot{x}, \dot{z}, \dot{\phi})^T =$

$$-\lambda \cdot \begin{pmatrix} 0.545 & -1.000 & -0.910 & 1.000 \\ -3.636 & 4.000 & 3.596 & -3.955 \\ -0.727 & 0.000 & 0.428 & -0.471 \end{pmatrix} \cdot \begin{pmatrix} X_1 + 1/4 \\ X_2 - 1/4 \\ Y_1 - 1/4 \\ Y_2 - 1/4 \end{pmatrix} \quad (15)$$

Finally, using relations (1), (2) and (15) we can derive the robot control vector $(\eta_1, \eta_2, \eta_3)^T$.

4.2 Homing on ceiling structures

The homing on ceiling structures uses passive vision. A grayscale camera is placed on top of the robot, so that the optical axis is vertical and the camera looks up to the ceiling (camera B in Figure 2). Assuming a ceiling parallel to the ground plane, the geometry of objects in the image is unaffected in size, which greatly simplifies image processing operations such as identifying and tracking occurrences of a predefined reference model. We use a vision system based on the IM-640 MATROX Image Series to track two references. The vision process time is about 150 ms.

The image features used for regulation are defined as the mass centers of the two tracked references. Similarly to the homing on landmark pairs, we have $\bar{s} = (X_1, X_2, Y_1, Y_2)^T$ and $\bar{s}^* = (-a, a, 0, 0)^T$. The matrix $\mathbf{L}_{\bar{s}\bar{s}^*}$ is derived from (4) and is equal to

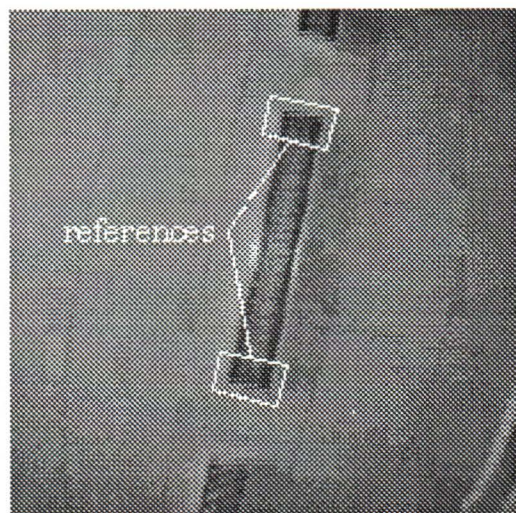


Figure 4 Predefined references of ceiling structures, such as lamps, are identified and tracked by a dedicated image processing system. Two references are used for homing the robot.

$$\begin{pmatrix} -1/z^* & 0 & -a/z^* & 0 & -1-a^2 & 0 \\ -1/z^* & 0 & a/z^* & 0 & -1-a^2 & 0 \\ 0 & -1/z^* & 0 & 1 & 0 & a \\ 0 & -1/z^* & 0 & 1 & 0 & -a \end{pmatrix} \quad (16)$$

Let us again consider a numerical example with $l = 1 m$ and $z^* = 2 m$. By keeping only relevant terms, the control law (11) may be simplified to $\dot{\bar{r}}_c = (\dot{x}, \dot{y}, \dot{\phi})^T =$

$$-\lambda \cdot \begin{pmatrix} -0.181 & -0.181 & 0.000 & 0.000 \\ 0.000 & 0.000 & -0.190 & -0.190 \\ 0.000 & 0.000 & 0.095 & 0.095 \end{pmatrix} \cdot \begin{pmatrix} X_1 + 1/4 \\ X_2 - 1/4 \\ Y_1 - 1/4 \\ Y_2 - 1/4 \end{pmatrix} \quad (17)$$

As before, we use relations (1), (2) and (15) to derive the robot control vector $(\eta_1, \eta_2, \eta_3)^T$.

4.3 Homing on wall corners

The homing on wall corners uses a grayscale video camera and a laser line-stripping system. The laser is placed at an angle with respect to the camera, so that the intersection of the laser stripe with wall corners in the scene creates two intersecting lines in the three-dimensional space (see Figure 5). Unlike other laser line-stripping vision



Figure 5 The robot is homing on a corner site using a horizontal laser line-stripe vision device, which trace is visible on the walls.

system that extract range data using triangulation methods, we are only interested in the image projection of the laser stripe intersection.

The laser stripe is described by the plane equation in the three-dimensional space

$$a_1x + b_1y + c_1z + d_1 = 0 \quad (18)$$

By using (6), (7) and (18), the functions $h_i(\bar{x}, \bar{p}^*)$ and $g_i(\bar{X}, \bar{P}^*)$ ($i = 1, 2$), associated to the two intersection lines, can be obtained at the desired camera pose (Espiau *et al.*, 1992). The latter is placed at a distance z^* on the line passing by the intersection of the two wall planes, parallel to the ground and at equal distance from them. For the image features, we choose $\bar{s} = (\psi_1, \rho_1, \psi_2, \rho_2)^T$, which yields $\bar{s}^* = (\psi_1^*, \rho_1^*, \psi_2^*, \rho_2^*)^T$ for the target image features.

The control law for the homing on corners is similar in form to that of (15).

5. EXPERIMENTAL RESULTS

The homing on landmark pairs we use in the self-positioning navigation is based on a two-steps implementation of (15): circling and translating. It is a preliminary evaluation of the vision-based control described in this paper, with the camera velocity limited to $(\dot{z}, \dot{\phi} = \dot{\theta})^T$. In a first step we fix the camera orientation with respect to the robot to $\phi = \theta + 90^\circ$, so that the robot moves on a circle in the ground plane, centered on the two landmarks. In a second step we fix $\phi = \theta$, so that the

robot moves on a line in the ground plane, passing in-between the two landmarks. An advantage of this implementation is that the dynamic model is simplified to

$$\begin{aligned} \eta_1 &= \dot{z} \\ \eta_2 = \eta_3 &= \dot{\phi} \end{aligned}$$

In this experimentation configuration, we use a fisheye lens to increase the camera field of view. This type of lens must normally be corrected by a non-linear term in the perspective projection, which is however relatively small near the image center. In practice, we observe that the radial distortion in the image has a tendency to accelerate convergence for initial conditions of $\bar{s}(\bar{r}_c, t)$ far away from the desired goal.

The results shown in Figure 6 present two examples of homing sequences using the two-steps method, where the X and Y axis correspond to the image features coordinates. The plots show the targets mass centers trajectories from $t = 0$ to $t = t_f$. The same results are presented differently in Figure 7, where two image features, X_1 and Y_1 , and their corresponding target image features, $X_1^* = -a$ and $Y_1^* = a$, are plotted against time.

The convergence of the homing control law is good, but the average time t_f for the homing sequence is relatively long. We are currently evaluating a direct implementation of the control law given by (15), which should decrease t_f without sacrificing convergence stability. The homing site center that corresponds to the final robot pose (fixed by \bar{s}^*) is repeatable within an uncertainty region of $7.8 \cdot 10^{-3} m^2$. Comparing this result to the robot size ($0.7 m$ diameter) and a capture zone size of about $15 m^2$ (region of the robot configuration space within which the image features are visible), the conclusion is that the homing precision is more than enough for mobile robot navigation using the self-positioning approach. More results on navigation are reported in (Facchinetti *et al.*, 1995).

6. CONCLUSION

We have presented homing behaviors that provide self-positioning of a mobile robot and constitute the key elements for the solution of a new navigation approach we presented in earlier publications. We proposed an analysis of three different homing configurations: homing on landmark pairs, homing on ceiling structures and homing on wall corners. Their control schemes are based

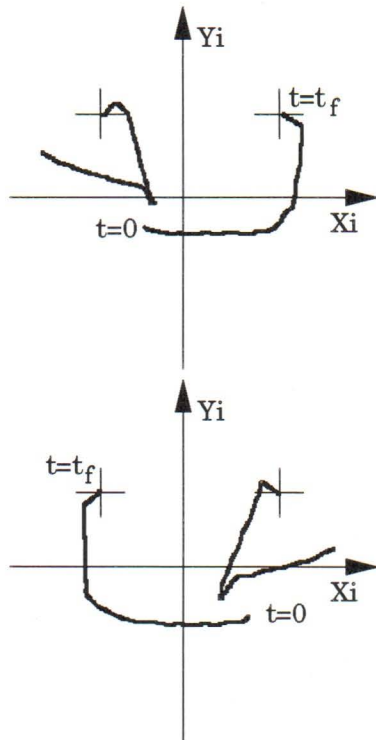


Figure 6 Results showing measured image features trajectories (target mass centers), as the homing on landmark pairs is performed from two different initial robot locations.

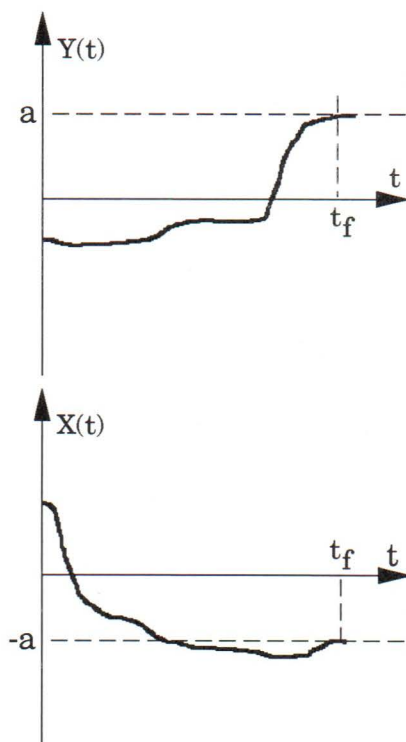


Figure 7 results showing two image features and their corresponding target image features versus time.

on regulation by image features and do not need a three-dimensional reconstruction of the scene with respect to the camera. Experimental results are reported for a preliminary implementation of the homing on landmark pairs, with a well-behaving control convergence. Based on these positive results, we are currently implementing the three vision-based homing behaviors into a full-blown self-positioning system for autonomous robot navigation.

Acknowledgements

This work is bound to project 4023-027037 of the Swiss National Research Program "Artificial Intelligence and Robotics" (NRP23), conducted in collaboration with the Institute of Informatics and AI of the University of Neuchâtel, Switzerland.

REFERENCES

- d'Andréa-Novel, B., Bastin, G., and Campion, G. (1991). Modelling and Control of Non-Holonomic Wheeled Mobile Robots. In: *Proc. of the IEEE Int. Conf. on Robotics and Automation*. pp. 1130-1135.
- Brooks, R.A. (1986). A robust layered control system for a mobile robot system. In: *IEEE Journal of Robotics and Automation*. Vol. RA-2, No. 1, pp. 14-23.
- Chacal B., J.A., and Sira-Ramírez, H. (1994). On the Sliding Mode Control of Wheeled Mobile Robots. In: *Proc. of the IEEE Int. Conf. on Systems, Man & Cybernetics*. pp. 1938-1943.
- Chantemargue, F., and Hügli, H. (1994). In: *Calculateurs Parallèles*. Vol. 6, No. 3, pp. 35-56.
- Chenavier, F., and Crowley, J.L. (1992). Position Estimation for a Mobile Robot Using Vision and Odometry. In: *Proc. of the IEEE Conf. on Robotics and Automation*. pp. 2588-2593.
- Connel, J.H., and Mahadevan, S. (1993). In: *Robot Learning*. Kluwer Academic Publishers, Boston.
- Dudek, G., Jenkin, M., Milios, G., and Wilkes, D. (1991). Robotic Exploration as Graph Construction In: *IEEE Transactions on Robotics and Automation*. Vol. 7, No. 6, pp. 859-865.
- Espiau, B., Chaumette, F., and Rives, P. (1992). A New Approach to Visual Servoing in Robotics. In: *IEEE Trans. on Robotics and Automation*. Vol. 8, No. 3, pp. 313-326.
- Facchinetti, C., Tièche, F., and Hügli, H. (1994). Using and Learning Vision-Based Self-Positioning for Autonomous Robot Navigation. In: *Proc. of the Int. Conf. on Machine Learning. Workshop on Robot Learning*, pp. 57-64.
- Facchinetti, C., Tièche, F., and Hügli, H. (1995). Using and Learning Vision-Based Self-Positioning for Autonomous Robot Navigation. To be published in: *Proc. of the Third Int. Conf. on Automation, Robotics and Computer Vision*. Singapore.
- Faugeras, O. (1993). In: *Three-Dimensional Computer Vision: A Geometric Viewpoint*. MIT Press, Massachusetts.
- Hügli, H., Tièche, F., Chantemargue, F., and Maitre, G. (1993). Architecture of an experimental vision-based robot navigation system. In: *Proc. of Swissvision*. Zurich, Switzerland, pp. 53-60.

- Kuipers, B.J., and Byun, Y.-T. (1991). A robot exploration and mapping strategy based on semantic hierarchy of spatial representations. In: *Journal of Robotics and Autonomous Systems*.
- Müller, J.-P., Hügli, H., Facchinetti, C., Tièche, F., Rodriguez, M., and Gat, Y. (1994). Architecture Of An Autonomous System: Application To Mobile Robot Navigation. In: *Proc. of the 2nd NRP 23 - Symposium on Artificial Intelligence and Robotics*. Lausanne, Switzerland, pp. 97-110.
- Pissard-Gibollet, R., and Rives, P. (1991). Asservissement visuel appliqué à un robot mobile: état de l'art et modélisation cinématique. In: *INRIA, Rapport de Recherche*. No. 1577.
- Samson, C., Le Borgne, M., and Espiau, B. (1991). Robot Control: The Task Function Approach. In: *Clarendon Press, Oxford*.
- Takeda, H., Facchinetti, C., and Latombe, J.-C. (1994). Planning the Motions of a Mobile Robot in a Sensory Uncertainty Field. In: *IEEE Transactions on Pattern Analysis and Machine Intelligence*. October issue, pp. 1002-1017.
- Tan, J.H.X., Pinette, B., Weiss, R. Riseman, E.M. (1991). Image-based Homing. In: *Proc. of the IEEE Int. Conf. on Robotics and Automation*. pp. 620-625.
- Tièche, F., Facchinetti, C., and Hügli, H. (1994). A Multi-Layered Hybrid Architecture To Solve Complex Tasks of an Autonomous Mobile Robot. In: *Proc. of the Third Golden West Int. Conf. on Intelligent Systems*. Las Vegas, USA.